# Au@MoS$_2$@WS$_2$ Core−Shell Architectures: Combining Vapor Phase and Solution-Based Approaches

Jennifer G. DiStefano, Akshay A. Murthy, Chamille J. Lescott, Roberto dos Reis, Yuan Li, and Vinayak P. Dravid*

Cite This: *J. Phys. Chem. C* 2020, 124, 2627−2633
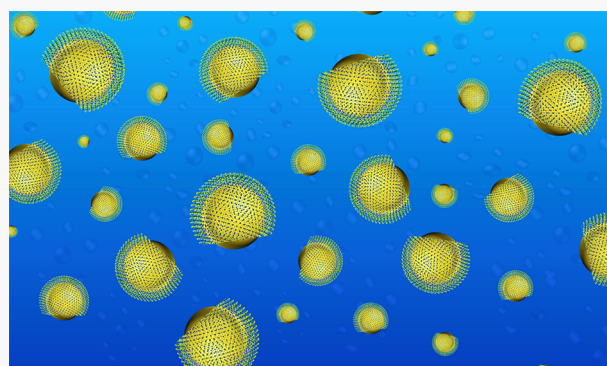
Read Online

ACCESS | 📊 Metrics & More | 📰 Article Recommendations | 🆘 Supporting Information

**ABSTRACT:** Solution preparation provides a versatile platform to extend the applications of transition-metal dichalcogenides (TMDs) beyond those achievable with traditional vapor-based preparation methods. However, existing solution-based synthesis and exfoliation approaches present numerous challenges, including low-crystallinity material and incompatibility with complex geometries, particularly with respect to spatial control over interfacial regions. Perhaps interestingly, these disadvantages align well with some of the advantages of vapor phase synthesis. Here, we introduce a strategy that combines vapor phase deposition and solution chemistry to build TMD core−shell heterostructures housed in aqueous media and reap the benefits of both preparation methods. We report a new TMD core−shell heterostructure, Au@MoS$_2$@WS$_2$, with an Au nanoparticle core and MoS$_2$ and WS$_2$ shells and provide a means of suspending the structure in solution to allow for higher order patterning and ligand-based functionalization. High-resolution electron microscopy and Raman spectroscopy provide a detailed analysis of the structure and interfaces of the core−shell heterostructures. UV−vis, dynamic light scattering, and zeta potential measurements exhibit outstanding natural stability and monodispersity of Au@MoS$_2$@WS$_2$ in solution. As a proof of concept, the aqueous environment is utilized to both functionalize the core−shell heterostructures with electrostatic ligands and pattern them into desired configurations on a target substrate. This work harnesses the advantages of vapor phase preparation of nanomaterials and the functionality possible with aqueous suspension to expand future engineering and application opportunities of TMD heterostructures.

Suspension of transition-metal dichalcogenides (TMDs) in solution has enabled attractive and unique engineering capabilities and spurred the development of numerous solution preparation methods. The many variations of wet chemical synthesis and exfoliation provide access to a wide array of TMD nanosheets suspended in solution.[1−7] In addition to the typical low cost and scalability of these solution preparation methods, they facilitate several powerful and unique opportunities for nanoscale control and engineering of TMDs, namely, (1) chemical functionalization; (2) hybridization with other functional nanomaterials; and (3) deposition and directed assembly on target substrates.[8] This accessibility and manipulation of TMDs possible in solution opens the door for multiple new technologies. Solution preparation of TMDs has benefited exploratory biomedical applications ranging from diagnostics to therapy.[9,10] Functionalized TMDs can serve as antibacterial agents[11] and chemotherapy drug-carriers,[12] and TMDs hybridized with plasmonic nanoparticles serve as a potent photothermal cancer treatment.[13] Additionally, a variety of fields including electrocatalysis,[14,15] sensing,[16,17] and battery technologies[18,19] have progressed due to functionalization and hybridization of TMDs in solution. Further, facile deposition of solution-prepared TMDs allows nanofabrication on

substrates not amenable to traditional high-temperature synthesis, enabling an array of flexible devices including battery electrodes,[18] gas sensors,[20] memory devices,[21] and data-storage devices.[22]

Despite the numerous attractive possibilities enabled by solution-prepared TMDs, their utility has been curtailed by several notable limitations. Wet chemical synthesis suffers from inherently low processing temperatures, yielding lower TMD quality than vapor phase techniques, and solution exfoliation often produces flakes of limited size, eliminating many downstream applications.[8,23] Additionally, preparation of multiple layered materials simultaneously cannot be controllably achieved with current solution-based methods, especially if certain geometries or ordering are desired. For instance, though some methods are capable of forming MoS$_2$/WS$_2$ hybrids from solution, they have historically lacked spatial
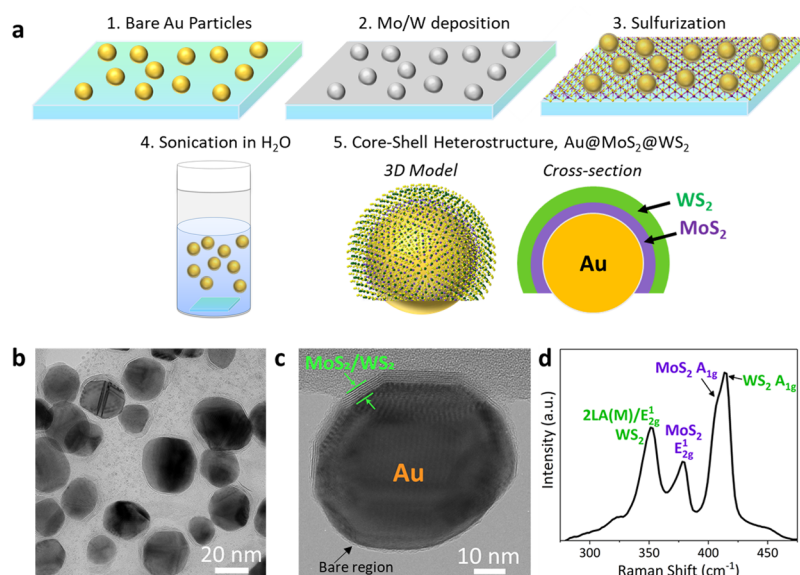
**Figure 1.** Growth schematic and structure demonstration of Au@MoS$_2$@WS$_2$ core−shell heterostructures. (a) Synthesis schematic depicting Mo and W metal deposition on Au nanoparticles followed by sulfurization to form MoS$_2$ and WS$_2$. Via bath sonication, the particles are then transferred to water to create an aqueous suspension of core−shell heterostructures. (b) Low-magnification TEM image of core−shell heterostructures. (c) High-magnification TEM of a single Au@MoS$_2$@WS$_2$ structure where the lamellar TMD shell is visible around the Au nanoparticle core. A bare surface of the core is labeled, which is where the particle contacted the substrate during deposition. (d) Raman spectrum indicating the presence of both expected TMDs.

control over interfacial regions.[24] Without the ability to precisely manipulate these interfaces, semiconducting heterostructures and the accompanying quantum phenomena cannot be engineered and utilized in applications such as high-performance electronics. However, vapor-phase synthesis methods can readily produce highly crystalline TMDs and provide precise interfacial control, such as formation of lateral or vertical TMD heterostructures. By controllably introducing a vapor-phase-synthesized material into solution, the advantages of each method can be accessed to maximize the potential of TMD structures.

In this study, we combine vapor phase deposition and solution chemistry to overcome these challenges and present a new TMD core−shell heterostructure suspended in water. We introduce a vapor phase thermal conversion method to produce the core−shell heterostructure Au@MoS$_2$@WS$_2$, where an Au nanoparticle is encapsulated by both MoS$_2$ and WS$_2$ shells. We employ the Au nanoparticle core as a vehicle to transport and suspend the surrounding MoS$_2$ and WS$_2$ layers in solution. We present data showing the unique structure of these core−shell heterostructures and high crystallinity of the TMD shells. Core−shell heterostructures in aqueous solution demonstrate the critical attributes of stability and mono-dispersity needed to exploit their properties, despite their lack of stabilizing ligands. Additionally, we utilize the solution environment to modify and control these nanostructures, specifically through chemical functionalization and patterning on a new substrate. This work leverages the superior material quality and control of vapor phase synthesis and the myriad of functionalization and patterning opportunities of solutions to produce colloidal suspensions of unique Au@MoS$_2$@WS$_2$ core−shell heterostructures.

## ■ RESULTS & DISCUSSION

Au@MoS$_2$@WS$_2$ core−shell heterostructures are synthesized using a modified thermally assisted conversion technique (Figure 1a). Au nanoparticle cores are produced by evaporating 6 nm of Au onto an SiO$_2$/Si substrate, followed by an 850 °C anneal to form particles across the substrate. Next, a 0.5 nm layer of Mo is deposited on the prepared substrate via electron beam evaporation, followed by a 0.5 nm layer of W. Finally, the substrate is sulfurized in a tube furnace to convert the Mo and W metals to MoS$_2$ and WS$_2$, respectively. An atomic force microscopy (AFM) image of the sulfurized layers is available in Figure S1. Figure S2 provides a scanning electron microscopy (SEM) image of the core−shell particles on their original growth substrate, with a mean diameter of 33 ± 7 nm. The substrate is then sonicated in water to transfer the particles to aqueous solution. A schematic of the final core−shell heterostructure is shown in Figure 1a.

Transmission electron microscopy (TEM) and Raman spectroscopy elucidate the structure and morphology of the core−shell particles. Figure 1b,c shows high-resolution TEM (HRTEM) images of core−shell heterostructures. The low-magnification image (Figure 1b) shows several encapsulated Au nanoparticles, and the TMD shell thickness is evident in Figure 1c where approximately six layers of TMD shells are visible along the top of the particle. The structures often exhibit a small bare region where the TMD shell does not cover the core, as evident along the bottom surface of the particle in Figure 1c. This exposed Au surface introduces additional functionality into this structure, as will be discussed later and can be attributed to the directionality inherent in electron beam deposition and the resultant lack of complete transition metal coverage. Additionally, Raman spectroscopy demonstrates the presence of each individual TMD. The Raman spectrum shown in Figure 1d exhibits the expected A$_{1g}$ (out-of-plane) and E$^1_{2g}$ (in-plane) vibration modes of both MoS$_2$ and WS$_2$ and the WS$_2$ 2LA(M) mode which overlaps with the E$_{2g}^1$.[25]
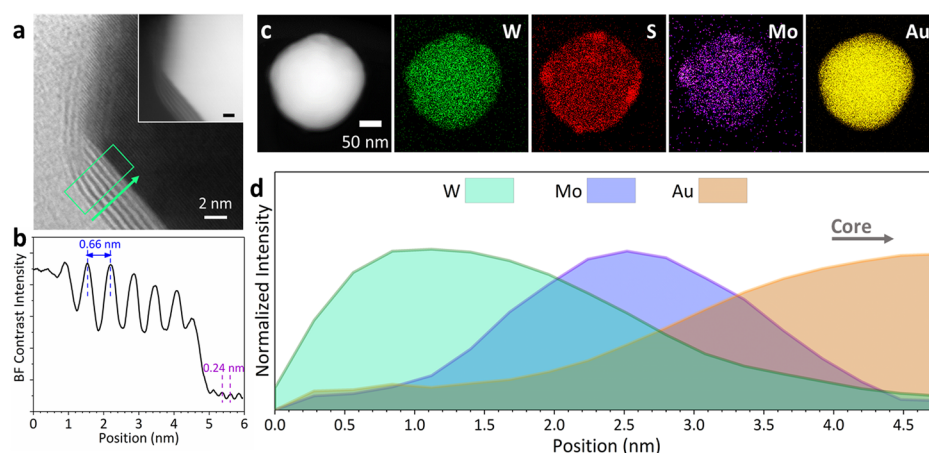
**Figure 2.** Compositional analysis of Au@MoS$_2$@WS$_2$ using STEM−EDS. (a) ABF STEM image of the core−shell heterostructure where the lattice fringes of the TMD shell are evident. Inset: Corresponding ADF image (scale bar 2 nm). (b) Contrast intensity line profile taken from the region of a green box in (a) in the direction of the arrow. Distance between peaks provides the TMD layer separation of 0.66 nm and Au lattice spacing of 0.24 nm, as expected. (c) EDS maps of an Au@MoS$_2$@WS$_2$ particle showing the reference image, W, S, Mo, and Au maps, respectively. (d) EDS line profile indicating the transition from shell to core.
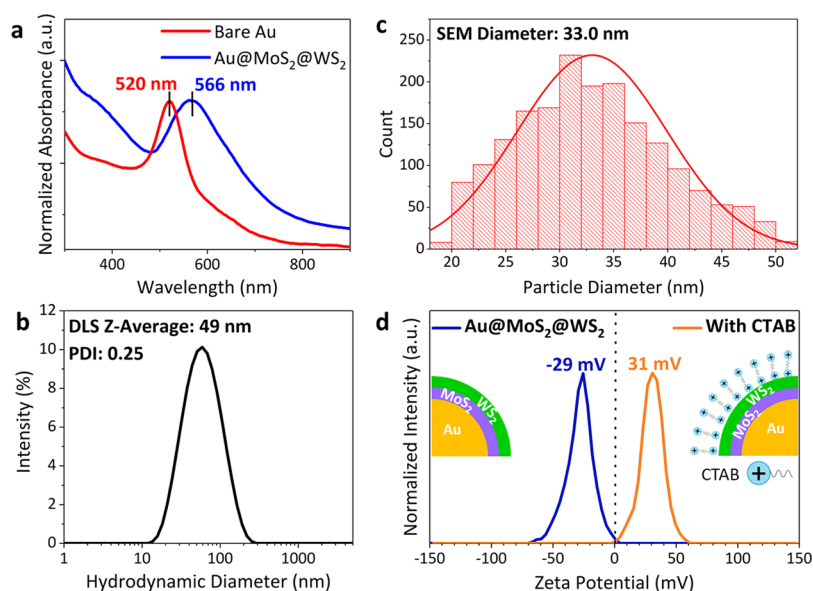


**Figure 3.** Solution characterization and functionalization of Au@MoS$_2$@WS$_2$. (a) UV−vis spectra comparing bare Au nanoparticles to core−shell heterostructures. The shift in the Au LSPR is indicative of a change in the dielectric environment caused by the surrounding MoS$_2$ and WS$_2$ layers and supports that the ensemble encapsulation is achieved. (b) Dynamic light scattering (DLS) measurement of the core−shell heterostructures in water reports a Z-average diameter of 49 nm and PDI of 0.25. (c) SEM size distribution of core−shell heterostructures provides a mean diameter of 33 nm. This value agrees with the DLS data once the difference in the measurement is accounted for, supporting that the core−shell heterostructures are monodisperse and do not aggregate in aqueous solution. (d) Zeta potential measurements of unfunctionalized Au@MoS$_2$@WS$_2$ and functionalized with cetyltrimethylammonium bromide (CTAB). Without functionalization, the core−shell heterostructures exhibit an impressively negative zeta potential. This negative repulsion between particles in solution likely explains the stability observed in DLS. Additionally, we observe the zeta potential with CTAB to be 31 mV, indicating CTAB attachment to the core−shell surface and successful functionalization.

To further examine the TMD shell structure, scanning TEM (STEM) is employed. The contrast in STEM imaging in annular bright-field (ABF) and annular dark-field (ADF) is nominally sensitive and proportional to atomic number Z and can therefore be used to precisely determine layer separation in the shell.[26] Figure 2b shows a contrast intensity profile from the reference ABF image in Figure 2a. In ABF images, higher Z elements appear darker due to electron absorption effects. In this structure, the brighter lines of the shell (peaks in the contrast intensity profile) correspond to the van der Waals gaps between TMD layers, and the darker lines correspond to

the heavier elements Mo and W (valleys in the contrast line profile). The separation between layers is approximately 0.66 nm. This closely matches the expected spacing between neighboring basal planes of MoS$_2$ and WS$_2$ and confirms that the Mo and W have indeed been sulfurized.[27,28] As the STEM contrast intensity profile extends into the core, a second set of oscillations appears corresponding to the lattice fringes of the {111} planes of Au.

Next, we employed STEM−energy dispersive X-ray spectroscopy (EDS) to gain local chemical information about the core−shells. The EDS elemental color maps shown in Figure

2c provide full-particle views of the chemical composition. These data confirm the coverage of the Au particle with Mo, W, and S, thus demonstrating the spatial distribution of each element is as expected. To examine the interface between materials, we conducted EDS line scans. The transition from the shell to the Au core is shown in Figure 2d, with the reference STEM image in Figure S3. Starting at the edge of the shell and moving in the direction of the core, we observe a notable increase in the W signal, corresponding to the $WS_2$ shell. As the W signal decreases, the Mo signal rises and eventually reaches its maximum, denoting the transition to $MoS_2$ as the innermost TMD. Au then becomes the most prominent element as the core is approached. More details about this analysis can be found in the Supporting Information.

While the exploration of other core−shell heterostructures is not the focus of this current work, we believe it is important to note the versatility of this core−shell synthesis method. We demonstrate the structural design opportunities by building core−shell superlattice particles, where the TMD shells alternate between $MoS_2$ and $WS_2$ (Figure S4). The demonstration of this structure exhibits the potential of this methodology to generate complex TMD heterostructures for suspension in solution moving forward.

Properties of plasmonic nanoparticles are particularly sensitive to their surrounding environment, including surface coatings and proximity to other particles. We can leverage this sensitivity of the Au nanoparticle cores to understand the ensemble structure and behavior of Au@$MoS_2$@$WS_2$ particles in aqueous solution. According to Mie theory,[29] the Au-localized surface plasmon resonance (LSPR) wavelength, which can be readily measured using UV−vis spectroscopy, will red-shift as the local refractive index increases.[30] Based on this, we expect the LSPR of the core−shell particles in solution to be red-shifted compared to that of bare Au particles surrounded by only water, due to the high index of refraction of TMDs.[31,32] Indeed, the core−shell heterostructures are observed to cause a red-shift in the Au LSPR peak location from 520 nm for bare Au nanoparticles to 566 nm for the core−shell heterostructures (Figure 3a). This shift is corroborated by previous absorbance calculations we reported on a 5-layer $MoS_2$ shell around Au particles.[33] These results indicate that the core−shell nanoparticles experience an altered dielectric environment due to $MoS_2$ and $WS_2$ shells and that ensemble encapsulation is achieved.

In addition to confirming ensemble encapsulation, the Au LSPR can also indicate the stability of a colloidal suspension. Aggregation of plasmonic particles, in our case Au, leads to coupling between neighboring particles and a notable red-shift in LSPR, the extent of which is dependent on the degree of aggregation.[34] This is often observed in UV−vis as a decrease in the expected LSPR intensity, attributed to fewer dispersed particles, and emergence of a lower energy secondary peak as the particles form aggregates.[35] Given the lack of such features in our spectra and previously stated agreement with prior calculations, the UV−vis measurements suggest the Au@$MoS_2$@$WS_2$ particles remain dispersed in water with no evidence of aggregation.

To further assess the stability of the Au@$MoS_2$@$WS_2$ solutions, we utilized DLS, a hydrodynamic size measurement technique. By measuring the size of species in the solution, we can determine both the dispersity of the particles and presence of contaminants. DLS reported a Z-average diameter and polydispersity index (PDI) of 49 nm and 0.25, respectively.

The size distribution from DLS is shown in Figure 3b, and SEM particle size measurements are shown in Figure 3c for reference. It is important to note that DLS measures hydrodynamic size and therefore cannot be expected to exactly match the SEM size values (see Supporting Information for detailed explanation); however, the shape of the distributions provide information about the state of the solution. The DLS data indicate that solutions can be produced with no unwanted contaminants, which would manifest as additional peaks (typically at larger sizes) visible in the size distribution (see Supporting Information S.1.3). Similarly, the formation of large Au@$MoS_2$@$WS_2$ aggregates in solution would also result in an extra peak. We can further look to the PDI value of the distribution to rule out the formation of small nanoparticle aggregates.[36] The PDI approximates the average uniformity of particles in solution on a scale from 0 to 1, where a PDI of zero represents a monodisperse solution comprised of perfectly uniform particles.[37] As such, a high PDI (>0.4) would indicate either a very broad particle size distribution or aggregation. Our reported PDI of 0.25 is well within the expected range of 0.1−0.4, considered "moderate polydispersity".[38] We expect some level of polydispersity simply because the size of the particles is not completely homogeneous, as evident by the SEM size distribution. Therefore, the combination of these two size measurement techniques indicates that the core−shell heterostructures are stable and do not aggregate in aqueous solution. This further corroborates our observations from UV−vis that the core−shell heterostructures form a monodisperse suspension.

This monodispersity of Au@$MoS_2$@$WS_2$ in aqueous solution is somewhat surprising given that no external stabilizing ligands are attached to the nanoparticle surfaces. TMD sheets in aqueous solution typically require stabilization by surfactants or surface receptors to prevent aggregation.[39] To investigate the origin of stability of core−shell heterostructures, we measured the surface charge of particles in solution using zeta potential. Interestingly, we find the zeta potential to be very negative (Figure 3d), suggesting that electrostatic repulsion between particles is the stabilizing mechanism of these solutions. The zeta potential of the core−shell solutions approaches the −30 mV threshold generally indicative of a stable solution.[39] We hypothesize this large surface charge may be linked to the retention of excess negative charge in few-layer TMD geometries, as other groups have reported previously.[40−42] This natural stability provides the additional advantage that the particle surface is a clean template, which can be directly functionalized for applications without the need for ligand exchange with stabilizing surfactants.

The natural stability and monodispersity of the Au@$MoS_2$@$WS_2$ solution makes it an ideal platform for accessing the modification and manipulation opportunities of solution preparation, namely functionalization, hybridization, and assembly. Chemical functionalization can provide the additional functionality necessary to make these solutions viable for future avenues such as programmable assembly and biomedical applications. We tested the potential for chemical functionalization of these particles using the electrostatic linker CTAB. The large positive charge inherent to CTAB molecules allows for the stabilization of particles in solution through repulsion of nearby particles and is detectable using a zeta potential measurement.[43] Figure 3d shows the zeta potential of CTAB-functionalized Au@$MoS_2$@$WS_2$ particles, following dialysis to remove excess CTAB, compared to the unfunctionalized

particles. The addition of CTAB causes a significant positive shift in the zeta potential, as expected, confirming successful surface functionalization.

The ability to functionalize core−shell heterostructures offers a powerful lever to control particle chemistry and placement. For example, CTAB itself can provide a simple route to self-assemble nanoparticles. As a solution of CTAB-functionalized nanoparticles dries, capillary forces drive the nanoparticles to assemble into a monolayer or various exotic patterns, which paves a route for facile patterning of the Au@MoS$_2$@WS$_2$ system that does not rely on advanced nano-fabrication processes.[44] The library of potential functionalizing molecules could be notably expanded through the inclusion of covalently bound molecules by exploiting the thiol chemistry opportunities of the WS$_2$ outer shell. The exposed Au surface will be particularly useful to enable strong, directional binding to a substrate or other particles by leveraging its strong affinity to sulfur. One could even imagine utilizing ligand-directed self-assembly to construct artificial crystals or site-specific patterns using Au@MoS$_2$@WS$_2$ as building blocks.

Further, particles in solution possess the distinct advantage over substrate-bound materials that they can be controllably patterned or hierarchically assembled onto a host of target substrates. This may serve as a particularly valuable approach to employ core−shell heterostructures as building blocks in a variety of future devices, where both the pattern design and type of the substrate provide unique functionality. The stability and monodispersity of core−shell heterostructures in solution, which are critical prerequisites to patterning, enable us to provide a proof-of-concept demonstration that Au@MoS$_2$@WS$_2$ can indeed be controllably patterned into arbitrary configurations from solution. SEM images of core−shell heterostructures patterned using electron beam lithography are provided in Figure 4a with the corresponding high-



**Figure 4.** Patterning Au@MoS$_2$@WS$_2$ particles from solution. (a) SEM image of core−shell heterostructures assembled into patterns using electron-beam lithography. (b) High-magnification SEM from the blue box region in (a) showing nanoparticles comprising a pattern. (c) MoS$_2$ Raman map of the pattern. (d) WS$_2$ Raman map of the pattern. Raman maps were generated using the respective E$_{2g}^1$ Raman signals for each TMD.

magnification image revealing the individual nanoparticles in Figure 4b. To confirm the presence and homogeneity of MoS$_2$ and WS$_2$ comprising this pattern, Raman maps of each are provided (Figure 4c,d). The Raman maps were constructed by selecting the respective E$_{2g}^1$ modes corresponding to each TMD. This proof-of-concept demonstrates promise that these

core−shell heterostructures can be precisely patterned from aqueous solution onto arbitrary substrates for future optoelectronic, sensing, and flexible devices.

## ■ SUMMARY & CONCLUSIONS

We report a new TMD core−shell preparation route to create stable colloidal suspensions of high quality, complex TMD architectures. S/TEM analysis confirms the unusual structural and compositional makeup of Au@MoS$_2$@WS$_2$ particles. Using UV−vis, DLS, and zeta potential measurements, we find that the core−shell heterostructures are stable and monodisperse in aqueous solution due to significant negative surface charge. We demonstrate the advantages of core−shell heterostructures in solution by showing CTAB functionalization and patterning on a new substrate. However, these are only a few examples of the many functionalization, hybridization, and assembly opportunities available with solution preparation of MoS$_2$/WS$_2$ heterostructures. The ability to attach electrostatic or thiol-based molecules to these particles provides a large parameter space of chemistries that can be employed for specific applications and sophisticated patterning. Further, the particles themselves can be customized based on design needs. Not only can the type and number of TMD layers be altered, but this structure provides a "built-in" hybridization opportunity where the core material could be selected based on desired properties for even more tunability. The core material could additionally be removed, depending on the application, to leave a standalone TMD shell, opening yet another avenue of exploration.[45] We believe this study provides the groundwork for extensive future manipulation and modification of core−shell heterostructures, extending their use to unique applications only achievable with colloidal suspension.

## ■ ASSOCIATED CONTENT

### ⓈI Supporting Information

The Supporting Information is available free of charge at https://pubs.acs.org/doi/10.1021/acs.jpcc.9b11365.

Experimental methods, further discussion on STEM−EDS and DLS results, supplementary figures of the AFM, SEM, and STEM line scan reference image, superlattice HRTEM, and additional patterns (PDF)
EDS line profile (XLSX)

## ■ AUTHOR INFORMATION

### Corresponding Author

**Vinayak P. Dravid** − *Northwestern University, Evanston, Illinois;* ⓞ orcid.org/0000-0002-6007-3063; Email: v-dravid@northwestern.edu

### Other Authors

**Jennifer G. DiStefano** − *Northwestern University, Evanston, Illinois;* ⓞ orcid.org/0000-0002-8829-0692
**Akshay A. Murthy** − *Northwestern University, Evanston, Illinois;* ⓞ orcid.org/0000-0001-7677-6866
**Chamille J. Lescott** − *Northwestern University, Evanston, Illinois*
**Roberto dos Reis** − *Northwestern University, Evanston, Illinois*
**Yuan Li** − *Northwestern University, Evanston, Illinois*
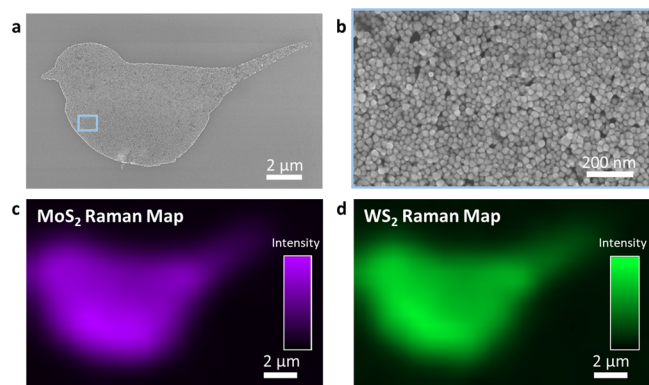
Complete contact information is available at:

## ■ REFERENCES

(1) Wang, P.-p.; Sun, H.; Ji, Y.; Li, W.; Wang, X. Three-Dimensional Assembly of Single-Layered MoS₂. *Adv. Mater.* **2014**, *26*, 964−969.

(2) Altavilla, C.; Sarno, M.; Ciambelli, P. A Novel Wet Chemistry Approach for the Synthesis of Hybrid 2D Free-Floating Single or Multilayer Nanosheets of MS₂@oleylamine (M=Mo, W). *Chem. Mater.* **2011**, *23*, 3879−3885.

(3) Han, J. H.; Kwak, M.; Kim, Y.; Cheon, J. Recent Advances in the Solution-Based Preparation of Two-Dimensional Layered Transition Metal Chalcogenide Nanostructures. *Chem. Rev.* **2018**, *118*, 6151−6188.

(4) Coleman, J. N.; Lotya, M.; O'Neill, A.; Bergin, S. D.; King, P. J.; Khan, U.; Young, K.; Gaucher, A.; De, S.; Smith, R. J.; Shvets, I. V.; Arora, S. K.; Stanton, G.; Kim, H.-Y.; Lee, K.; Kim, G. T.; Duesberg, G. S.; Hallam, T.; Boland, J. J.; Wang, J. J.; Donegan, J. F.; Grunlan, J. C.; Moriarty, G.; Shmeliov, A.; Nicholls, R. J.; Perkins, J. M.; Grieveson, E. M.; Theuwissen, K.; Mccomb, D. W.; Nellist, P. D.; Nicolosi, V. Two-Dimensional Nanosheets Produced by Liquid Exfoliation of Layered Materials. *Science* **2011**, *331*, 568−571.

(5) Smith, R. J.; King, P. J.; Lotya, M.; Wirtz, C.; Khan, U.; De, S.; O'Neill, A.; Duesberg, G. S.; Grunlan, J. C.; Moriarty, G.; Chen, J.; Wang, J.; Minett, A. I.; Nicolosi, V.; Coleman, J. N. Large-Scale Exfoliation of Inorganic Layered Compounds in Aqueous Surfactant Solutions. *Adv. Mater.* **2011**, *23*, 3944−3948.

(6) Zheng, J.; Zhang, H.; Dong, S.; Liu, Y.; Tai Nai, C.; Suk Shin, H.; Young Jeong, H.; Liu, B.; Ping Loh, K. High Yield Exfoliation of Two-Dimensional Chalcogenides Using Sodium Naphthalenide. *Nat. Commun.* **2014**, *5*, 2995.

(7) Nicolosi, V.; Chhowalla, M.; Kanatzidis, M. G.; Strano, M. S.; Coleman, J. N. Liquid Exfoliation of Layered Materials. *Science* **2013**, *340*, 1226419.

(8) Zhang, X.; Lai, Z.; Tan, C.; Zhang, H. Solution-Processed Two-Dimensional MoS₂ Nanosheets: Preparation, Hybridization, and Applications. *Angew. Chem., Int. Ed.* **2016**, *55*, 8816−8838.

(9) Cheng, L.; Liu, J.; Gu, X.; Gong, H.; Shi, X.; Liu, T.; Wang, C.; Wang, X.; Liu, G.; Xing, H.; Bu, W.; Sun, B.; Liu, Z. PEGylated WS₂ Nanosheets as a Multifunctional Theranostic Agent for in Vivo Dual-Modal CT/Photoacoustic Imaging Guided Photothermal Therapy. *Adv. Mater.* **2014**, *26*, 1886−1893.

(10) Yuan, Y.; Li, R.; Liu, Z. Establishing Water-Soluble Layered WS₂ Nanosheet as a Platform for Biosensing. *Anal. Chem.* **2014**, *86*, 3610−3615.

(11) Karunakaran, S.; Pandit, S.; Basu, B.; De, M. Simultaneous Exfoliation and Functionalization of 2H-MoS₂ by Thiolated Surfactants: Applications in Enhanced Antibacterial Activity. *J. Am. Chem. Soc.* **2018**, *140*, 12634−12644.

(12) Liu, T.; Wang, C.; Gu, X.; Gong, H.; Cheng, L.; Shi, X.; Feng, L.; Sun, B.; Liu, Z. Drug Delivery with PEGylated MoS₂ Nano-Sheets for Combined Photothermal and Chemotherapy of Cancer. *Adv. Mater.* **2014**, *26*, 3433−3440.

(13) Maji, S. K.; Yu, S.; Chung, K.; Ramasamy, M. S. Synergistic Nanozymetic Activity of Hybrid Gold Bipyramid− Molybdenum Disulfide Core@Shell Nanostructures for Two-Photon Imaging and Anticancer Therapy. *ACS Appl. Mater. Interfaces* **2018**, *10*, 42068.

(14) Huang, X.; Zeng, Z.; Bao, S.; Wang, M.; Qi, X.; Fan, Z.; Zhang, H. Solution-Phase Epitaxial Growth of Noble Metal Nanostructures on Dispersible Single-Layer Molybdenum Disulfide Nanosheets. *Nat. Commun.* **2013**, *4*, 1444.

(15) Youn, D. H.; Han, S.; Kim, J. Y.; Kim, J. Y.; Park, H.; Choi, S. H.; Lee, J. S. Highly Active and Stable Hydrogen Evolution Electrocatalysts Based on Molybdenum Compounds on Carbon Nanotube−Graphene Hybrid Support. *ACS Nano* **2014**, *8*, 5164−5173.

(16) Nandwana, V.; Huang, W.; Li, Y.; Dravid, V. P. One-Pot Green Synthesis of Fe₃O₄/MoS₂ 0D/2D Nanocomposites and Their Application in Noninvasive Point-of-Care Glucose Diagnostics. *ACS Appl. Nano Mater.* **2018**, *1*, 1949−1958.

(17) Kim, J.-S.; Yoo, H.-W.; Choi, H. O.; Jung, H.-T. Tunable Volatile Organic Compounds Sensor by Using Thiolated Ligand Conjugation on MoS₂. *Nano Lett.* **2014**, *14*, 5941−5947.

(18) David, L.; Bhandavat, R.; Singh, G. MoS₂/Graphene Composite Paper for Sodium-Ion Battery Electrodes. *ACS Nano* **2014**, *8*, 1759−1770.

(19) Chen, Y.; Lu, J.; Wen, S.; Lu, L.; Xue, J. Synthesis of SnO₂/MoS₂ Composites with Different Component Ratios and Their Applications as Lithium Ion Battery Anodes. *J. Mater. Chem. A* **2014**, *2*, 17857−17866.

(20) He, Q.; Zeng, Z.; Yin, Z.; Li, H.; Wu, S.; Huang, X.; Zhang, H. Fabrication of Flexible MoS₂ Thin-Film Transistor Arrays for Practical Gas-Sensing Applications. *Small* **2012**, *8*, 2994−2999.

(21) Liu, J.; Zeng, Z.; Cao, X.; Lu, G.; Wang, L.-H.; Fan, Q.-L.; Huang, W.; Zhang, H. Preparation of MoS₂-Polyvinylpyrrolidone Nanocomposites for Flexible Nonvolatile Rewritable Memory Devices with Reduced Graphene Oxide Electrodes. *Small* **2012**, *8*, 3517−3522.

(22) Tan, C.; Qi, X.; Liu, Z.; Zhao, F.; Li, H.; Huang, X.; Shi, L.; Zheng, B.; Zhang, X.; Xie, L.; Tang, Z.; Huang, W.; Zhang, H. Self-Assembled Chiral Nanofibers from Ultrathin Low-Dimensional Nanomaterials. *J. Am. Chem. Soc.* **2015**, *137*, 1565−1571.

(23) Manzeli, S.; Ovchinnikov, D.; Pasquier, D.; Yazyev, O. V.; Kis, A. 2D Transition Metal Dichalcogenides. *Nat. Rev. Mater.* **2017**, *2*, 17033.

(24) Jeffery, A. A.; Nethravathi, C.; Rajamathi, M. Two-Dimensional Nanosheets and Layered Hybrids of MoS₂ and WS₂ through Exfoliation of Ammoniated MS₂ (M = Mo,W). *J. Phys. Chem. C* **2014**, *118*, 1386−1396.

(25) Berkdemir, A.; Gutiérrez, H. R.; Botello-Méndez, A. R.; Perea-López, N.; Elías, A. L.; Chia, C.-I.; Wang, B.; Crespi, V. H.; López-Urías, F.; Charlier, J.-C.; Terrones, H.; Terrones, M. Identification of Individual and Few Layers of WS₂ Using Raman Spectroscopy. *Sci. Rep.* **2013**, *3*, 1755.

(26) Findlay, S. D.; Shibata, N.; Sawada, H.; Okunishi, E.; Kondo, Y.; Ikuhara, Y. Dynamics of Annular Bright Field Imaging in Scanning Transmission Electron Microscopy. *Ultramicroscopy* **2010**, *110*, 903−923.

(27) Gutiérrez, H. R.; Perea-López, N.; Elías, A. L.; Berkdemir, A.; Wang, B.; Lv, R.; López-Urías, F.; Crespi, V. H.; Terrones, H.;

Terrones, M. Extraordinary Room-Temperature Photoluminescence in Triangular $WS_2$ Monolayers. *Nano Lett.* **2013**, *13*, 3447−3454.

(28) Lee, C.; Yan, H.; Brus, L. E.; Heinz, T. F.; Hone, J.; Ryu, S. Anomalous Lattice Vibrations of Single- and Few-Layer $MoS_2$. *ACS Nano* **2010**, *4*, 2695−2700.

(29) Mie, G. Beiträge Zur Optik Trüber Medien, Speziell Kolloidaler Metallösungen. *Ann. Phys.* **1908**, *330*, 377−445.

(30) Liz-Marzán, L. M.; Giersig, M.; Mulvaney, P. Synthesis of Nanosized Gold−Silica Core−Shell Particles. *Langmuir* **1996**, *12*, 4329−4335.

(31) Yim, C.; O'Brien, M.; McEvoy, N.; Winters, S.; Mirza, I.; Lunney, J. G.; Duesberg, G. S. Investigation of the Optical Properties of $MoS_2$ Thin Films Using Spectroscopic Ellipsometry. *Appl. Phys. Lett.* **2014**, *104*, 103114.

(32) Jung, G.-H.; Yoo, S.; Park, Q.-H. Measuring the Optical Permittivity of Two-Dimensional Materials without a Priori Knowledge of Electronic Transitions. *Nanophotonics* **2019**, *8*, 263−270.

(33) DiStefano, J. G.; Li, Y.; Jung, H. J.; Hao, S.; Murthy, A. A.; Zhang, X.; Wolverton, C.; Dravid, V. P. Nanoparticle@$MoS_2$ Core−Shell Architecture: Role of the Core Material. *Chem. Mater.* **2018**, *30*, 4675−4682.

(34) Norman, T. J.; Grant, C. D.; Magana, D.; Zhang, J. Z.; Liu, J.; Cao, D.; Bridges, F.; Van Buuren, A. Near Infrared Optical Absorption of Gold Nanoparticle Aggregates. *J. Phys. Chem. B* **2002**, *106*, 7005−7012.

(35) Shipway, A. N.; Lahav, M.; Gabai, R.; Willner, I. Investigations into the Electrostatically Induced Aggregation of Au Nanoparticles. *Langmuir* **2000**, *16*, 8789−8795.

(36) Filipe, V.; Hawe, A.; Jiskoot, W. Critical Evaluation of Nanoparticle Tracking Analysis (NTA) by NanoSight for the Measurement of Nanoparticles and Protein Aggregates. *Pharm. Res.* **2010**, *27*, 796−810.

(37) Clayton, K. N.; Salameh, J. W.; Wereley, S. T.; Kinzer-Ursem, T. L. Physical Characterization of Nanoparticle Size and Surface Modification Using Particle Scattering Diffusometry. *Biomicrofluidics* **2016**, *10*, 054107.

(38) Bhattacharjee, S. DLS and Zeta Potential − What They Are and What They Are Not? *J. Controlled Release* **2016**, *235*, 337−351.

(39) Gupta, A.; Arunachalam, V.; Vasudevan, S. Water Dispersible, Positively and Negatively Charged $MoS_2$ Nanosheets: Surface Chemistry and the Role of Surfactant Binding. *J. Phys. Chem. Lett.* **2015**, *6*, 739−744.

(40) Heising, J.; Kanatzidis, M. G. Exfoliated and Restacked $MoS_2$ and $WS_2$: Ionic or Neutral Species? Encapsulation and Ordering of Hard Electropositive Cations. *J. Am. Chem. Soc.* **1999**, *121*, 11720−11732.

(41) Voiry, D.; Goswami, A.; Kappera, R.; Silva, C. d. C. C. e.; Kaplan, D.; Fujita, T.; Chen, M.; Asefa, T.; Chhowalla, M. Covalent Functionalization of Monolayered Transition Metal Dichalcogenides by Phase Engineering. *Nat. Chem.* **2015**, *7*, 45−49.

(42) Knirsch, K. C.; Berner, N. C.; Nerl, H. C.; Cucinotta, C. S.; Gholamvand, Z.; McEvoy, N.; Wang, Z.; Abramovic, I.; Vecera, P.; Halik, M.; Sanvito, S.; Duesberg, G. S.; Nicolosi, V.; Hauke, F.; Hirsch, A.; Coleman, J. N.; Backes, C. Basal-Plane Functionalization of Chemically Exfoliated Molybdenum Disulfide by Diazonium Salts. *ACS Nano* **2015**, *9*, 6018−6030.

(43) Wang, H.; Kundu, J.; Halas, N. J. Plasmonic Nanoshell Arrays Combine Surface-Enhanced Vibrational Spectroscopies on a Single Substrate. *Angew. Chem., Int. Ed.* **2007**, *46*, 9040−9044.

(44) Sau, T. K.; Murphy, C. J. Self-Assembly Patterns Formed upon Solvent Evaporation of Aqueous Cetyltrimethylammonium Bromide-Coated Gold Nanoparticles of Various Shapes. *Langmuir* **2005**, *21*, 2923−2929.

(45) Chen, X.; Yang, H.; Liu, G.; Gao, F.; Dai, M.; Hu, Y.; Chen, H.; Cao, W.; Hu, P.; Hu, W. Hollow Spherical Nanoshell Arrays of 2D Layered Semiconductor for High-Performance Photodetector Device. *Adv. Funct. Mater.* **2018**, *28*, 1705153.